Talanta 276 (2024) 126293

Contents lists available at ScienceDirect

Talanta

journal homepage: www.elsevier.com/locate/talanta

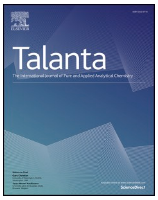

Rapid and simple viral protein detection by functionalized 2D MoS_2/graphene electrochemiluminescence aptasensor

Laura Gutiérrez-Gálvez [a], Hanaa El Hajioui-El Ghalbzouri [a], Estefanía Enebral-Romero [a,b], Marina Garrido [b], Alicia Naranjo [b], David López-Diego [c], Mónica Luna [c], Emilio M. Pérez [b], Tania García-Mendiola [a,d,**], Encarnación Lorenzo [a,b,d,*]

[a] *Departamento de Química Analítica y Análisis Instrumental, Universidad Autónoma de Madrid, 28049, Madrid, Spain*
[b] *IMDEA-Nanociencia, Ciudad Universitaria de Cantoblanco, 28049, Madrid, Spain*
[c] *Instituto de Micro y Nanotecnología IMN-CNM, CSIC (CEI UAM+CSIC), Isaac Newton 8, Tres Cantos, 28760, Madrid, Spain*
[d] *Institute for Advanced Research in Chemical Sciences (IAdChem), Universidad Autónoma de Madrid, 28049, Madrid, Spain*

ARTICLE INFO

Keywords:
Electrochemiluminescence
Aptasensor
Covalently linked 2D heterostructures
Electrografting
SARS-CoV-2

ABSTRACT

In this work we present the development of an electrochemiluminescence aptasensor based on electrografting molybdenum disulphide nanosheets functionalized with diazonium salt (MoS_2–N_2^+) upon screen-printed electrodes of graphene (SPEs GPH) for viral proteins detection. In brief, this aptasensor consists of SPEs GPH electrografted with MoS_2–N_2^+ and modified with a thiolated aptamer, which can specifically recognize the target protein analyte. In this case, we have used SARS-CoV-2 spike protein as model protein. Electrochemiluminescence detection was performed by using the $[Ru(bpy)_3]^{2+}$/TPRA (tripropylamine) system, which allows the specific detection of the SARS-CoV-2 spike protein easily and rapidly with a detection limit of 9.74 fg/mL and a linear range from 32.5 fg/mL to 50.0 pg/mL. Moreover, the applicability of the aptasensor has been confirmed by the detection of the protein directly in human saliva samples. Comparing our device with a traditional saliva antigen test, our aptasensor can detect the spike protein even when the saliva antigen test gives a negative result.

1. Introduction

Over the past three decades, there have been hundreds of thousands of deaths caused by regular outbreaks of viral diseases [1]: severe acute respiratory syndrome coronavirus (SARS-CoV) in 2003, influenza A virus H1N1 subtype in 2009, Zika virus (ZIKV) in 2014, middle east respiratory syndrome coronavirus (MERS-CoV) in 2014, Ebola virus (EBOV) in 2014 and severe acute respiratory syndrome coronavirus 2 (SARS-CoV-2) in 2019. This last outbreak led to the recent COVID-19 pandemic. During this pandemic the importance of rapid virus detection has been highlighted, as it minimizes the spread of the virus and, therefore, the morbidity and mortality. For this reason, we selected SARS-CoV-2 as model virus to perform this work.

At the beginning of the COVID-19 pandemic, computerized tomography (CT) scan, and poly-chain reaction (PCR) were very popular, but over time, due to the high transmission rate of the disease, the need arose for rapid and cheap diagnostic tests with significant sensitivity and specificity. In this context, a universal interest in the development of biosensors, specifically based on nanomaterials, has emerged for the real-time virus detection [2].

Biosensors consist of a biological or biomimetic recognition element, whose function is to recognize a part of the virus, and a transducer to convert said recognition event into a detectable signal. Specifically, biorecognition elements could be whole cells, enzymatic reactions, products of the patient's immune response system such as antibodies and genetic material from viruses such as DNA and RNA [3]. An emerging method to detect SARS-CoV-2 is based on the use of an aptamer as recognition element [4]. An aptamer is a single-stranded DNA or RNA molecule which can bind to targets by folding into a 3D structure [5]. Unlike antibodies, aptamers can be chemically synthesized, at lower cost, and modified with high stability and little batch-to-batch variation [4,5]. Due to their high affinity and specificity,

---

* Corresponding author. Departamento de Química Analítica y Análisis Instrumental, Universidad Autónoma de Madrid, 28049, Madrid, Spain.
** Corresponding author. Departamento de Química Analítica y Análisis Instrumental, Universidad Autónoma de Madrid, 28049, Madrid, Spain.
E-mail addresses: tania.garcia@uam.es (T. García-Mendiola), encarnacion.lorenzo@uam.es (E. Lorenzo).

https://doi.org/10.1016/j.talanta.2024.126293
Received 21 February 2024; Received in revised form 7 May 2024; Accepted 19 May 2024

aptamers have been applicated in the development of therapies and diagnostic tools for some pathogens such as bacteria [6–8], parasites [9,10], and viruses [4,11,12]. Therefore, taking into account the huge interest from the scientific community in the development of new SARS-CoV-2 detection tools, several aptasensors has been published for the detection of this virus [13–26]. However, there is still a great deal of interest in the development of new device with improved performance. In fact, none of them are based on the use of the ultrasensitive analytical technique called electrochemiluminescence (ECL).

ECL is a powerful transduction technique [27], which consists of the emission of light by excited species through high-energy electron transfer reactions. This technique combines the advantages of chemiluminescence and electrochemical techniques and allows obtaining spatially localized signals and controlling the reaction through the application of electrode potential. On the other hand, it offers high sensitivity because it presents an exceptionally low background signal [28]. The combination of this technique with nanomaterials allows the achievement of new and improved sensitive detection platforms. Hence, the electrode surface modification with nanomaterials (nanostructuration) improves the sensing performance due to it allows the enhancement of the electrode surface area, facilitates the biorecognition elements immobilization, decreases the non-specific binding sites and enhances the electron transfer in catalytic reactions [29]. With this purpose, most published works use previously synthesized nanomaterials to modify electrodes and develop biosensors rather than “in situ” nanomaterials synthesis on the electrode surface. Nevertheless, the procedures traditionally used to prepare these electrodes require complicated steps, such as coating the electrode surface, drying at higher temperatures, and mixing with binders. Among the different methods to deposit nanomaterials onto electrode surfaces for biosensor fabrication, the drop-casting “manual deposition” method is the most extensively used due to its ease and simplicity. However, this method usually utilizes binders as dimethylformamide or polyvinyl alcohol, among others, with nanomaterials to firmly modify the electrode surfaces [30] that inevitably blocks catalytic active sites, affects the electrolyte diffusion and increases the series resistance, which leads to poor reproducibility, low stability, and reduced electrocatalytic activity [31–34]. Hence, a nanomaterial deposition method that is stable, facile and reproducible is essential to achieve high performance designed biosensors [29]. In this sense, the covalent attachment of nanomaterials onto the electrode surface can open a new emerging area of improved biosensing devices. Even though most air-stable 2D materials are relatively inert, many strategies have been developed for their covalent modification [35–39]. Particularly, the reactivity of MoS_2 depends on its polytype, being less reactive the semiconducting (2H–MoS_2) than the metallic one (1T-MoS_2). An optimal approach for chemically modifying these materials should be mild, avoiding the introduction of numerous defects, while also being versatile to accommodate the attachment of a wide variety of functional groups. More specifically, using maleimides for the covalent functionalization of MoS_2 has been shown as a mild, fast and versatile protocol [40–42], where functionalization occurs under room temperature, in less than 1 h and in different solvents. Besides, in this type of functionalization has been proved that no changes in phase are needed (from 2H to 1T) because the modification occurs under mild conditions in the semiconducting 2H phase. In those regards, the covalent functionalization of MoS_2 with a maleimide diazonium salt (MoS_2–N_2^+) has been proposed to build a 2D covalent heterostructure electrode made with graphene and MoS_2 nanosheets, as some of us previously reported [23]. Briefly, the soft nucleophilic sulfur atoms present in the MoS_2 surface react with the double bond of maleimide compounds, in a “click” type thiol-ene reaction [36,40]. Once it is attached to MoS_2, the dangling diazonium salt (present in the maleimide compound) offers the perfect reacting group for attaching the functionalized MoS_2 to graphene [43].

Hence, the 2D covalent heterostructure electrode made with graphene and MoS_2 nanosheets can be an interesting alternative to develop more stable, facile, and reproducible biosensors. Additionally, as it is well-established, the use of nanomaterials improves the analytical performance of these devices, so the implementation of this 2D covalent heterostructure in the biosensor design allows the possibility of benefit the synergy of both nanomaterials [23]. In addition, the 2D heterostructure can be used as a novel immobilization platform of biorecognition elements as thiolated molecules can interact with the basal plane of MoS_2 due to its strong interaction in its reduced (thiol) or oxidized (disulfide) form [38,44–47]. Therefore, this platform in combination with the outstanding ECL technique results in a promising strategy for the sensitive detection of analytes of clinical interest.

Based on the better performance that a modified electrode built with a MoS_2/graphene covalent heterostructure can provide in the development of sensing devices, in this work we present a novel electrochemiluminescence aptasensor for the detection of viral proteins based on this type of modified electrodes.

2. Material and methods

2.1. Chemicals

A synthetic DNA aptamer (SH-Apt) of 51 nucleotides long which specifically recognize the receptor-binding domain (RBD) of the SARS-CoV-2 spike protein used in this work was purchased from Merk (www.merckgroup.com/es-es). This aptamer was modified in the 5′extreme with an hexalquilthiol (5′–SH–$(CH_2)_6$):

5′–SH–$(CH_2)_6$-CAGCACCGACCTTGTGCTTTGGGAGTGCT
GGTCCAAGGGCGTTAATGGACA-3′

Sodium phosphate dibasic dihydrate ($Na_2HPO_4 \cdot 2H_2O$), sodium phosphate monobasic monohydrate ($NaH_2PO_4 \cdot H_2O$), sodium chloride (NaCl), 1,4-Dithiothreitol (DTT), a NAP-10 column of Sephadex G-25, acetonitrile (CH_3CN; ACN), tripropylamine (TPrA), bovine serum albumin (BSA), antigen p53, immunoglobulin G (IgG), human carcinoembryonic antigen (CEA) and tris(2,2′-bipyridyl)dichlororuthenium(II) hexahydrate ($[Ru(bpy)_3]Cl_2 \cdot 6H_2O$) were provided by Merck (www.merckgroup.com/es-es). SARS-CoV-2 (2019-nCoV) Spike S1-His Recombinant Protein (S1) (HPLC-verified) (40,591-V08H), Influenza A H1N1 (A/California/04/2009) Hemagglutinin/HA Protein (ECD, His Tag) (11,055-V08H) and MERS-CoV Spike/S1 Protein (S1 Subunit, aa 1–725, His Tag) (40,069-V08B1) were provided by Sino Biological Europe GmbH (Eschborn, Germany). SARS-CoV-2 (COVID-19) Antigen Rapid Test (Saliva) for self-testing fabricated by Hangzhou AllTest Biotech Co., Ltd. (REF: ICOV–803H) were purchased from Suministros Generales para Laboratorio (SGL; https://sglab.net/). Bulk MoS_2 was purchased from Sigma Aldrich. *N*-(4-aminophenyl) maleimide, as a precursor for the formation of the diazonium salt, was bought from Apollo Scientific.

2.2. Instrumentation

Purified water Millipore Milli-Q-System (18.2 MΩ cm) was used in all experiments.

All material and solutions were sterilized in a Nüve OT012 autoclave before to be used.

Electrochemical and electrochemiluminescence (ECL) experiments were carried out using Metrohm screen-printed electrodes of graphene (DRP-110GPH; SPEs GPH), which integrate a carbon working electrode modified with graphene, a silver pseudo-reference electrode and a carbon auxiliary electrode.

With the aim of electrochemical characterize the aptasensor, an autolab (PGSTAT 30 potentiostat) from Metrohm was used. It was controlled with the software package GPES 4.9 or FRA using a screen-printed electrode connector (Metrohm).

The ECL experiments were carried out with a SpectroECL controlled with the specific software DropView SPELEC. This instrument has a bipotentiostat/galvanostat (±4 V potential range, ±40 mA maximum measurable current). A Metrohm DropSens Si-photodiode cell (DRP-ECLPHOTODIODCELL) was employed (spectral response range from 340 to 1100 nm). In the case of the spectroelectrochemiluminescence measurements, they were recorded with a Spectrometer Cell (wavelength range from 340 to 850 nm).

Atomic Force Microscopy (AFM) images were acquired with a Nanotec Electrónica AFM system, in jumping mode (one entire force curve is acquired at each measurement point), using silicon cantilevers (PPP-FM Nanosensors, 2.8 N/m nominal spring constant and 75 kHz resonant frequency in air) in air. WSxM software [48] was used for the acquisition and processing of images.

SEM and EDAX (Energy-dispersive X-ray analysis) images have been taken with FEI instrument (VERIOS 460).

Fourier-transform infrared spectroscopy with attenuated total reflection (FT-ATR-IR) was performed in a Bruker ALPHA FT-IR spectrometer.

The thermogravimetric analysis (TGA) was carried out by a TGA Q500 equipment, supplied by TA instruments, in air at a rate of 10 °C (from 100 to 800 °C), after an equilibrium isotherm at 50 °C for 15 min.

Raman measurements were carried out using a Bruker Senterra II confocal Raman microscope (Bruker Optic, Ettlingen, Germany, resolution 3–5 cm^{-1}) using 50× objective with an aperture of 0.75; 532 nm laser excitation and 2 mW.

2.3. Procedures

2.3.1. Synthesis of molybdenum disulphide functionalized with diazonium salt (MoS_2–N_2^+)

First, MoS_2 was exfoliated by liquid phase exfoliation (LPE) in *N*-Methyl-2-pyrrolidone (NMP), as reported by Pérez and co-workers [40]. Briefly, a 1 mg/mL suspension was sonicated using an ultrasonic probe for 1 h, at 35 % of amplitude. Then, centrifuged for 30 min at 5000 rpm and supernatant was filtered using PTFE membrane filters (0.45 μm). Exfoliated material was finally redispersed in acetonitrile (ACN) and washed several times under ACN and isopropanol (i-PrOH), obtaining the exfoliated pristine material (*p*-MoS_2).

The general procedure to obtain the functionalized material was also reported by Pérez and co-workers in previous works. Briefly, *N*-(4-diazophenyl) maleimide was firstly synthesized [43] and then solubilized into a 0.4 mg/mL *p*-MoS_2 suspension, under inert atmosphere. This mixture was stirred overnight at room temperature protected from light. Then, this suspension was filtered and washed with ACN, obtaining the functionalized material, MoS_2–N_2^+.

2.3.2. 1 mg/mL MoS_2–N_2^+ solution preparation

1 mg/mL MoS_2–N_2^+ dispersion was prepared just before to be used for the electrografting process. For that, 3 mg of the synthesized MoS_2–N_2^+ was suspended in 3 mL of ACN. Finally, the suspension was sonicated for 15 min.

2.3.3. Thiolated aptamer, BSA, and Spike protein solutions preparation

A 10.0 μM stock solution of the thiolated aptamer (SH-Apt) was prepared following the protocol for thiol-modified oligonucleotide reduction using 1,4-Dithiothreitol (DTT) and a NAP-10 column of Sephadex G-25.

0.1 % bovine serum albumin (BSA) solution was prepared just prior to be used. For this purpose, 10 mg of BSA was dissolved in 10 mL of 10 mM PB 0.4 M NaCl pH 7.0 (PBS). The obtained solution was subsequent filtered with a 0.45 μm nylon syringe filters.

Spike protein standard (stored at – 80 °C) was reconstituted at final concentration of 0.25 mg/mL. This solution was used for preparing a 1 ng/mL Spike protein stock (stored at – 20 °C) in PBS, which was prepared once a month. The diluted solutions of different concentrations of Spike protein used in this work were prepared from the 1 ng/mL stock in PBS just prior to be used.

2.3.4. ECL signal of $[Ru(bpy)_3]^{2+}$/TPrA system

ECL signals on SPE GPH or SPE GPH/MoS_2–N_2^+ were obtained by depositing 60.0 μL of a 7 mM $[Ru(bpy)_3]^{2+}$ solution with different concentrations of TPrA in 0.1 M PB pH 7.4. Then, a cyclic potential scan from 0.00 V to 1.90 V at 0.01 V/s was applied, obtaining electrochemical and ECL signals, both being registered at the same time.

2.3.5. Biosensor electrochemical characterization

Electrochemical impedance spectroscopy (EIS) and cyclic voltammetry (CV) techniques were used to characterize the different biosensor development steps. Both CV and EIS measurements were acquired in 10 mM $Fe(CN)_6^{3-}$ and 10 mM $Fe(CN)_6^{4-}$ (as redox probe) in 0.1 M PB pH 7.

Cyclic voltammograms were performed from −1.0 to 1.2 V (2 scans) at 100 mV/s. EIS was registered applying the following conditions: 0.12 V in the frequency range from 100 kHz to 0.01 Hz with 10 mV amplitude. The obtained EIS data were represented in a Nyquist plot (-Z'' vs. Z') and fitted to a Randles equivalent circuit that consists of the charge transfer resistance (R_{ct}), solution resistance (R_s), a Warburg impedance element (Z_W) and a constant phase element (CPE) that models the non-ideal behavior of the double layer capacitance.

2.3.6. Spike protein aptasensor development

2.3.6.1. Electrografting of MoS_2–N_2^+ on SPEs GPH surface.

SPE GPH were summitted to an electrografting process with molybdenum disulphide functionalized with diazonium salt (MoS_2–N_2^+) by applying 15 consecutive scans from −1.5 V to 1.0 V at 0.1 V/s in 1 mg/mL MoS_2–N_2^+ solution in ACN saturated with N_2. The process was performed in an electrochemical cell with reflux of water to avoid evaporation of ACN, obtaining the platform denoted as SPE GPH/MoS_2–N_2^+.

2.3.6.2. Thiolated aptamer immobilization upon SPE GPH/MoS_2–N_2^+ surface.

MoS_2–N_2^+/SPE GPH electrodes were dropcasted with 10.0 μL of 10.0 μM of thiolated aptamer (SH-Apt) and were kept at room temperature for 24 h (SH-Apt/MoS_2–N_2^+/SPE GPH).

2.3.6.3. Blocking with BSA.

10.0 μL of 0.1 % BSA (blocker agent) in PBS were added to SH-Apt/MoS_2–N_2^+/SPE GPH electrodes for 30 min for blocking non-specific absorptions [49], obtaining the platform Blocker/SH-Apt/MoS_2–N_2^+/SPE GPH. After that, it was washed with Milli-Q water to remove any unabsorbed material.

2.3.6.4. Incubation with Spike protein.

Finally, Blocker/SH-Apt/MoS_2–N_2^+/SPE GPH electrodes were incubated in humid chamber during 1 h at 37 °C with 10.0 μL of the analyte protein (Spike) and, finally, washed with Milli-Q water.

2.3.6.5. Electrochemiluminescence detection.

ECL emission was obtained by applying a cyclic potential scan from 0.00 V to 1.90 V at 0.01 V/s in 60.0 μL of 7 mM $[Ru(bpy)_3]^{2+}$ and 500 μM TPrA in 0.1 M PB pH 7.4. The produced ECL signal and cyclic voltammogram were registered at the same time. Finally, the ECL aptasensor response were normalized with the blank (Blocker/SH-Apt/MoS_2–N_2^+/SPE GPH) as a percentage:

$$Normalized\ ECL\ (\%) = \frac{(ECL\ signal - blank\ ECL\ signal)}{blank\ ECL\ signal} \cdot 100$$

The blank signal is recorded by performing at least 3 different biosensors per day. These measurements are carried out with independent sensors/electrodes prepared exclusively for this purpose. Table 1SI shows blank signals of different electrodes from different days.

2.3.6.6. Spike protein detection in spiked untreated human saliva samples.

To study the matrix effect and to corroborate the biosensor applicability, untreated human saliva samples spiked with Spike protein was used. These samples were prepared by using untreated saliva sample of a volunteer, which was spiked with Spike protein (from 0.10 to 50.00 pg/mL). After that, this solution (10.0 μL) was incubated in humid chamber (1 h at 37 °C) on Blocker/SH-Apt/MoS_2–N_2^+/SPE GPH electrodes and washed with Milli-Q water to remove unabsorbed material. The ECL detection was performed as is described above. Finally, the Spike protein concentration was calculated using the normalized ECL signal of the spiked human saliva sample.

3. Results and discussion

In this work we present a new electrochemiluminiscence aptasensor for the early diagnose of viral diseases, based on 2D MoS_2 functionalized with a diazonium salt and graphene electrodes, whose development steps are depicted in Scheme 1. Firstly, a screen-printed electrode of graphene (SPE GPH) was submitted to an electrografting process of molybdenum disulphide nanosheets functionalized with diazonium salt (MoS_2–N_2^+), obtaining a 2D heterostructure formed by graphene and MoS_2 nanosheets covalently linked (step 1). Upon this surface (MoS_2–N_2^+/SPE GPH), the thiolated aptamer (SH-Apt) is immobilized (SH-Apt/MoS_2–N_2^+/SPE GPH) (step 2) onto the basal plane of MoS_2 due to its strong interaction in its reduced (thiol) or oxidized (disulfide) form [38,44–47]. Next, the non-specific sites of the surface were blocked (step 3) with bovine serum albumin or BSA (blocker). Then, the resulting surface (Blocker/SH-Apt/MoS_2–N_2^+/SPE GPH) was subsequently incubated with the analyte (in this case, SARS-CoV-2 spike protein), reaching the final platform Spike/Blocker/SH-Apt/MoS_2–N_2^+/SPE GPH (step 4). Finally, the selective aptamer-protein binding is detected by measuring the changes of the anodic ECL signal of $[Ru(bpy)_3]^{2+}$ and tripropylamine (TPrA) before and after incubation with the analyte (step 5).

Based on Scheme 1 depicted above, the first step was the synthesis and characterization of the nanomaterials used.

3.1. *Synthesis and characterization of MoS_2–N_2^+*

The synthesis and functionalization of the different materials employed (from diazonium salt to MoS_2–N_2^+) is described in the experimental section, and more detailed in a previously published work [43].

For the characterization of the new batches (both pristine and functionalized, *p*-MoS_2 and MoS_2–N_2^+ respectively), thermogravimetric analysis (TGA) was performed to ensure the correct functionalization, (see Fig. 1SI). The quantification of the functionalization degree for MoS_2–N_2^+ was achieved by analysing TGA profiles of both species, where a weight loss difference of 8 % was found, corresponding to the molecules of diazonium maleimide attached to the MoS_2. Furthermore, Fourier-transform infrared spectroscopy with attenuated total reflection (FT-ATR-IR) was performed to support the TGA results. It was possible to observe the stretching band of the carbonyl of the succinamide at 1709 cm^{-1} and a new band related to the C–S bond arose at 690 cm^{-1}. Besides, the C–H bending of the alkene disappears after the reaction between the maleimide and *p*-MoS_2.

3.2. *Aptasensor development*

3.2.1. *Electrografting process of MoS_2–N_2^+*

The second step in the aptasensor development was the electrografting of molybdenum disulphide nanosheets functionalized with diazonium salt (MoS_2–N_2^+) on graphene screen-printed electrodes (SPE GPH), as was mentioned before and depicted in Scheme 1. The electrografting process was performed applying 15 consecutive scans of cyclic potential to the MoS_2–N_2^+ suspension. In this way, the diazonium salt is reduced and the aryl radical is formed, allowing the covalent bond formation between MoS_2–N_2^+ and graphene of the SPE GPH surface. The result is a 2D heterostructure formed by graphene and MoS_2 nanosheets covalently linked, as we previously described [23]. During this electrografting process, a non-electroactive layer is formed with the covalent anchoring of the diazonium salt upon the electrode surface, producing a hinder in the electron transfer and, therefore, a decrease in the current is observed with the number of scans [50] (see Fig. 2SI).

3.2.2. *ECL behaviour of the $[Ru(bpy)_3]^{2+}$/TPrA system upon the electrografted platform*

During the last 20 years, the $[Ru(bpy)_3]^{2+}$/TPrA ECL system has been widely employed in the biosensors' area [51]. However, this is the first time that the ECL signal of the $[Ru(bpy)_3]^{2+}$/TPrA system is recorded on MoS_2–N_2^+/SPE GPH. The "oxidative–reduction" coreactant ECL pathway mechanism of the $[Ru(bpy)_3]^{2+}$/TPrA system is well-known [52,53], which is represented upon our developed electrografted platform in Fig. 1A. With the purpose of confirming that the same mechanism is occurring upon MoS_2–N_2^+/SPE GPH, a 3D ECL spectrum of the $[Ru(bpy)_3]^{2+}$/TPrA system upon the MoS_2–N_2^+/SPE GPH platform was recorded. In Fig. 1B, an ECL emission peak centered at around 625 nm and 1.0 V can be observed. Therefore, the ECL emission can be attributed to the electronic transition of the excited state of $[Ru(bpy)_3]^{2+*}$ to $[Ru(bpy)_3]^{2+}$, due to the fluorescence spectra of the $[Ru(bpy)_3]^{2+}$ has a maximum centered at around that wavelength [54]. This experiment confirms that "oxidative–reduction" coreactant ECL pathway mechanism of the $[Ru(bpy)_3]^{2+}$/TPrA system is also happening in our developed platform.

Once the ECL mechanism is confirmed, we recorded the ECL signal (Fig. 1C) of 7 mM $[Ru(bpy)_3]^{2+}$ in absence of TPrA (red line) and with different concentrations of this correactant (0 μM (red curve), 50 μM (green curve), 100 μM (blue curve), 250 μM (cyan curve), 500 μM (purple curve) and 1000 μM (orange curve)) in 0.1 M PB pH 7.4 at MoS_2–N_2^+/SPE GPH. As it is expected, the ECL signal increases with the

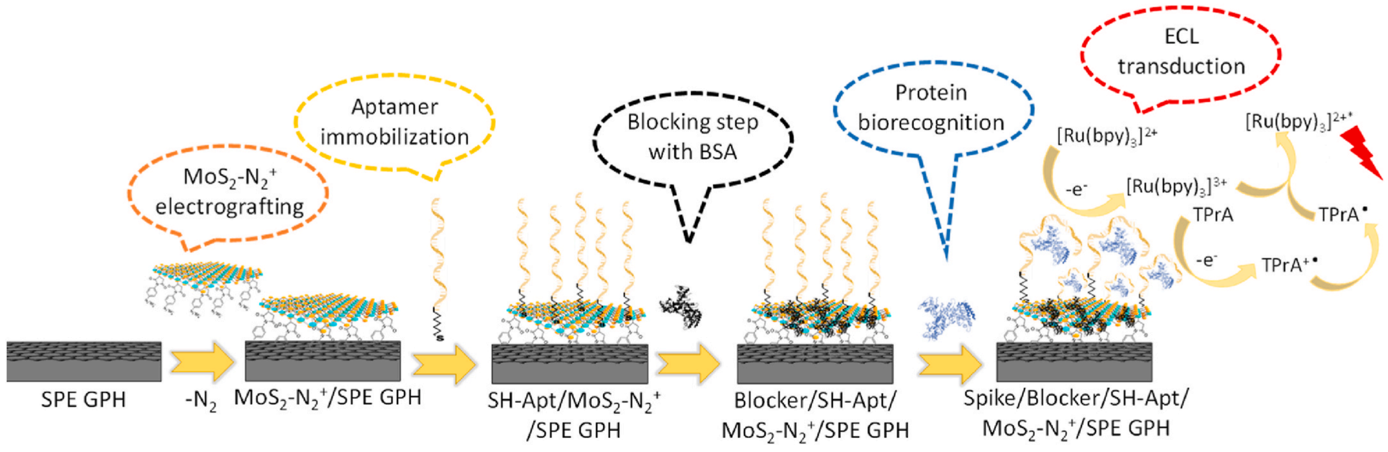

Scheme 1. 2D covalent MoS_2 and graphene heterostructure based-aptasensor design.

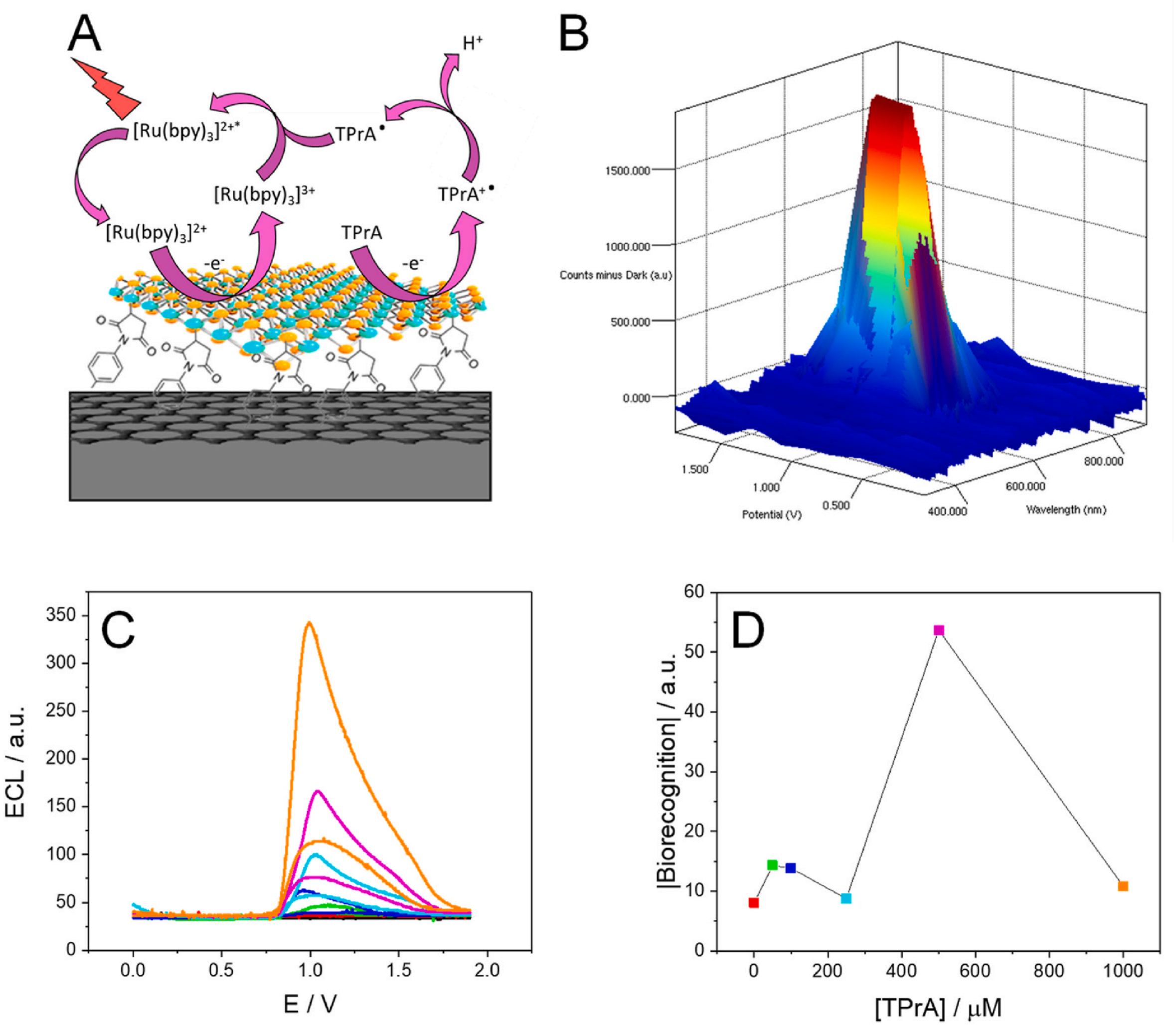

Fig. 1. (A) ECL mechanism of the $[Ru(bpy)_3]^{2+}$/TPrA system upon the electrografted platform MoS_2–N_2^+/SPE GPH. (B) 3D ECL spectrum of $[Ru(bpy)_3]^{2+}$/TPrA system at MoS_2–N_2^+/SPE GPH. (C) ECL signals of 7 mM $[Ru(bpy)_3]^{2+}$ with different concentration of TPrA: 0 μM (red curve), 50 μM (green curve), 100 μM (blue curve), 250 μM (cyan curve), 500 μM (purple curve) and 1000 μM (orange curve) in 0.1 M PB pH 7.4 (black curve) on MoS_2–N_2^+/SPE GPH. (D) Biorecognition signal of 5.00 pg/mL of Spike protein as a function of the TPrA concentration.

TPrA concentration. So, to decide which concentration of TPrA is the most optimal to develop the proposed aptasensor, we determined the absolute biorecognition signal (the signal of the entire platform Spike/Blocker/SH-Apt/MoS_2–N_2^+/SPE GPH minus the blank, which is the platform without analyte: Blocker/SH-Apt/MoS_2–N_2^+/SPE GPH) employing the different concentrations of TPrA previously employed. The best biorecognition was obtained by using 500 μM of TPrA. Therefore, the rest of the experiments was carried out with this optimized concentration of TPrA.

3.2.3. Aptasensor characterization

Once the MoS_2–N_2^+ is correctly electrografted upon the SPE GPH surface, the thiolated aptamer (SH-Apt) is immobilized (MoS_2–N_2^+/SPE GPH) due to the interaction of thiolated group and MoS_2 lattice [38, 44–47] (see Scheme 1). Then, in order to confirm the successful aptasensor development and to have a total control of the process in order to obtain reproducible results, each step followed in the development as well as the final device was deeply characterized by different techniques such Atomic Force Microscopy (AFM), Scanning Electron Microscopy (SEM) with energy dispersive X-ray spectroscopy analysis (EDAX),

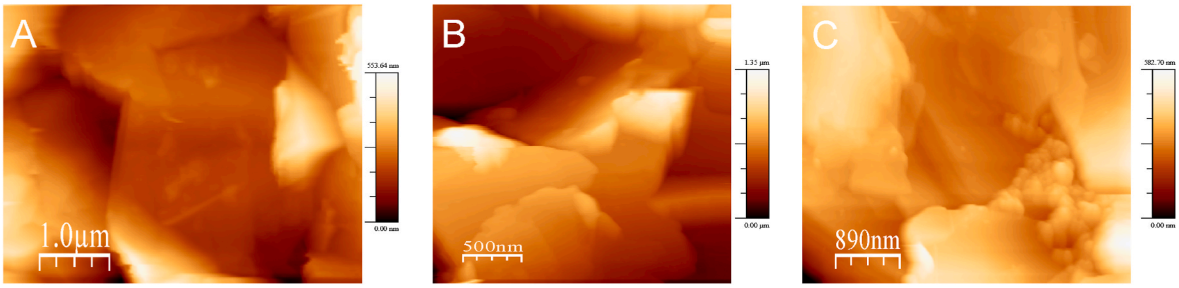

Fig. 2. AFM images of (A) SPE GPH, (B) MoS_2–N_2^+/SPE GPH and (C) SH-Apt/MoS_2–N_2^+/SPE GPH.

electrochemical impedance spectroscopy (EIS), X-Ray photoelectron spectroscopy (XPS) and Raman spectroscopy.

Fig. 2 shows the AFM surface characterization, which reveals the changes in the topographical height. The graphene flakes of the graphene screen-printed electrode (SPE GPH) can be clearly distinguished in the three different stages of the aptasensor building.

These three different stages in the construction of the aptasensor (bare SPE GPH, MoS_2–N_2^+/SPE GPH and SH-Apt/MoS_2–N_2^+/SPE GPH) were also characterized by SEM. Secondary electrons images (Fig. 3A, B, 3E, 3F, 3I and 3J) are useful for the inspection of the topography of the sample's surface while the backscattered electrons images (Fig. 3C, G and 3K) provide differences in the atomic number of materials placed on and below the surface of the sample. EDAX images obtained through SEM were also recorded (Fig. 3D, H and 3L). Considering this

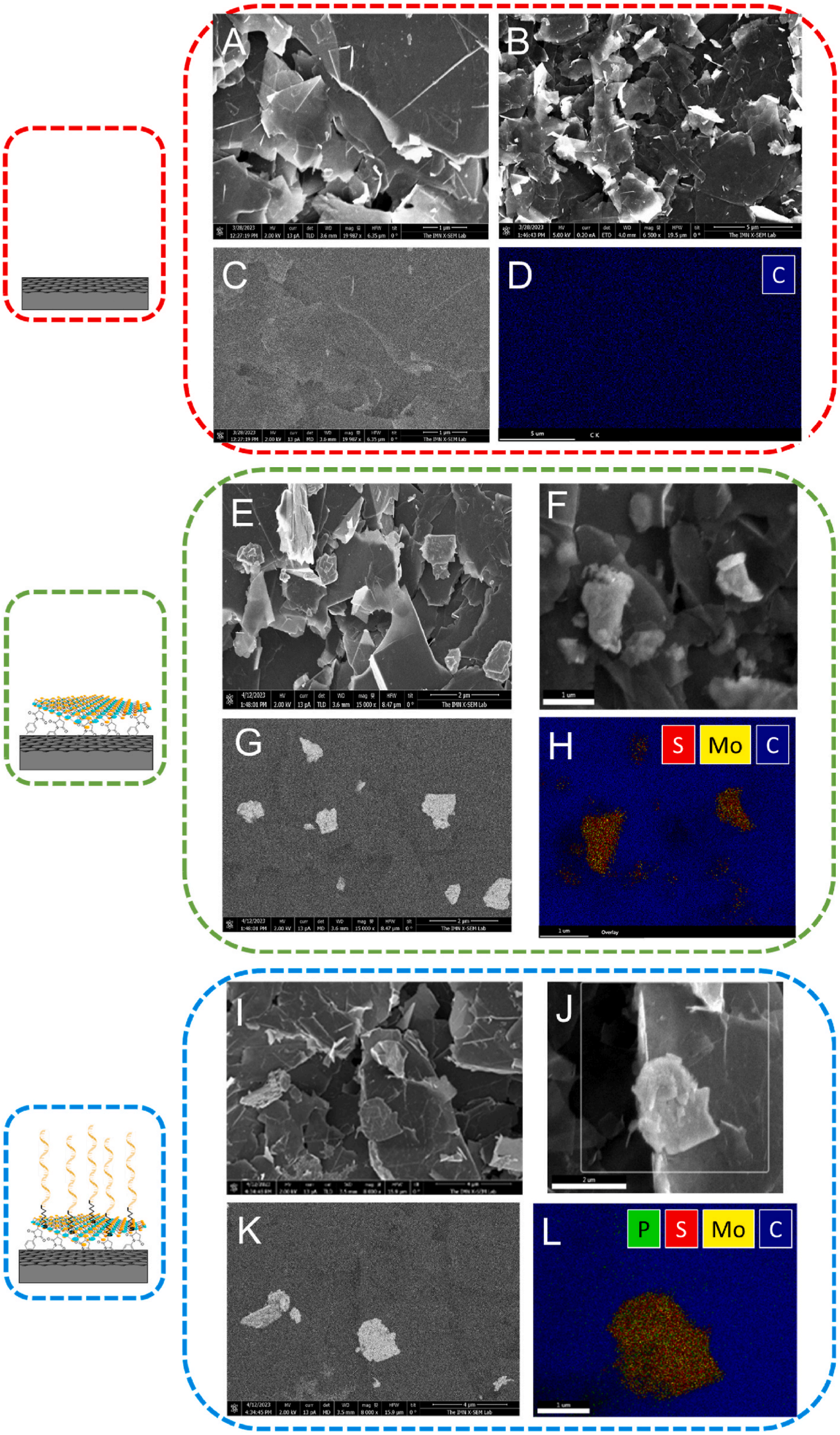

Fig. 3. SEM images of (A–D) SPE GPH, (E–H) MoS_2–N_2^+/SPE GPH and (I–L) SH-Apt/MoS_2–N_2^+/SPE GPH.

information, the analysis of the bare SPE GPH (Fig. 3A–D) shows the surface covered by just graphene flakes since the only element detected in the EDAX image is carbon (C). In addition, due to the absence of any element different from carbon, no contrast is observed in Fig. 3C and D. However, the presence of the MoS_2–N_2^+ nanosheets can be clearly distinguished in Fig. 3G and H (clear gray) from the SPE GPH (dark gray) in Fig. 3C and D, since Mo and S present higher atomic numbers than C. In this case, the EDAX image (Fig. 3H) also reveals the existence of molybdenum (Mo) and sulfur (S) together with carbon (C). These results point to SPE GPH nanostructuration with MoS_2–N_2^+ nanosheets. Regarding the immobilization of the thiolated aptamer (Fig. 3I–L), it could be easily confirmed by the EDAX image (Fig. 3L) which also shows the presence of phosphorus (P) on the surface, corresponding to the presence of DNA.

A further characterization of the biosensing platform was performed with CV and EIS using $Fe(CN)_6^{3-}/Fe(CN)_6^{4-}$ as redox probe. The results can effectively demonstrate the different modifications of the electrode [55]. The cyclic voltammogram (Fig. 3SIA) of $Fe(CN)_6^{3-}/Fe(CN)_6^{4-}$ at the bare SPE GPH (red curve) shows the characteristics oxidation and reduction peaks of the $Fe(CN)_6^{3-}/Fe(CN)_6^{4-}$ redox couple at 0.35 V and −0.072 V respectively, a peak-to-peak separation (ΔEp) of 422 mV and a peak current (I_p) of 330 μA. After carrying out the electrografting process of MoS_2–N_2^+ on SPE GPH (green curve), an increase in ΔE_p (439 mV) and a decrease in I_p (249 μA) are shown, which indicates hindering of electron transfer due to the formation of a less-electroactive layer on the electrode surface after the formation of a covalent bonding between the diazonium salt and the graphene of the electrode. After the electrode modification with the thiolated aptamer (blue curve), the ΔE_p and the I_p increases to 533 mV and decreases to 234 μA respectively, which indicates worsening of the electron transfer caused by the electrostatic repulsion between the negatively charged aptamer and the negative charge of the $Fe(CN)_6^{3-}/Fe(CN)_6^{4-}$ redox couple [56–58]. This confirms the aptamer immobilization on the MoS_2–N_2^+/SPE GPH surface. Finally, after surface blocking with the blocker agent (BSA) (purple curve), the reduction peak further shifted towards cathodic potentials, while the oxidation peak slightly shifted to a more positive potential ($\Delta Ep = 844$ mV) both with significantly lower current density ($I_p = 194$ μA), corroborating the effective blockage of the non-specific binding sites upon the electrode surface [57,58].

EIS was also registered with the aim of studying the interface properties of each electrode modification step [55]. The Nyquist plots obtained are represented in Fig. 3SIB, in which the diameter of each semi-circle equals to the electron-transfer resistance (R_{ct}) [55]. The Nyquist plots for the bare SPE GPH (red curve) and for the MoS_2–N_2^+/SPE GPH (green curve) show a R_{ct} of 43.95 Ω and 91.21 Ω, respectively. Thus, there is a worsening in the charge transfer after the formation of a non-electroactive layer during the electrografting process. After the electrode modification with the thiolated aptamer, as one would expect, the semicircle diameter increases reaching a value of 112.65 Ω (blue curve) due to the electrostatic repulsion between the $Fe(CN)_6^{3-}/Fe(CN)_6^{4-}$ redox couple and the also negatively charged aptamer layer [56–58], corroborating the successful aptamer immobilization on the MoS_2–N_2^+/SPE GPH. Finally, a further increase in the charge transfer resistance up to 139.23 Ω is shown in the purple curve, which corresponds to the Blocker/SH-Apt/MoS_2–N_2^+/SPE GPH electrode. Thus, after blocking the electrode surface with BSA, there is a hindering in the interfacial electron transfer that confirm the presence of BSA on the non-specific binding sites [57,58]. Therefore, CV results correspond to those obtained using EIS, corroborating the successful development of the aptasensor.

The XPS spectra of the bare SPE GPH (Fig. 3SIC, red curve) shows the C 1s signal from the electrode surface, as it consists of carbon electrodes modified with graphene as a carbon-based nanomaterial (www.dropsens.com; consulted on April 17, 2023). Once the MoS_2–N_2^+ is electrografted upon that surface (green curve), S 2p signal of the MoS_2–N_2^+ is observed, corroborating the presence of that nanomaterial in the electrode surface. Finally, after the aptamer immobilization on MoS_2–N_2^+/SPE GPH platform, the O 1s, N 1s, and P 2s/2p signals can be observed (blue curve), which corresponds to the nitrogenous bases of the thiolated aptamer sequence [59,60]. Thus, the aptamer immobilization is also confirmed.

Finally, Raman spectroscopy was also employed to confirm that the aptasensor has been successfully developed. As can be seen in Fig. 3SID, the spectrum of SPE GPH (red curve) presents the characteristics D, G, and 2D Raman bands (at 1350, 1581, and 2718 cm^{-1}, respectively) of the carbon present on the electrode surface. However, in the Raman spectrum of MoS_2–N_2^+/SPE GPH (green curve), another two bands appear at 380 cm^{-1} and 406 cm^{-1} that corresponds to the two active Raman modes E_{2g}^1 and A_{1g} of the molybdenum disulphide. Finally, in the SH-Apt/MoS_2–N_2^+/SPE GPH spectrum (blue curve), some peaks at 1000 cm^{-1} are observed, probably due to the nitrogenous bases of the thiolated DNA aptamer [60].

After deeply characterized the aptasensor development, we studied the ECL response of the final device. We compared this response to those recorded at the different steps followed in the aptasensor development. The ECL signals are represented in Fig. 4. As can be seen, there is a high ECL response at MoS_2–N_2^+/SPE GPH (green curve), that dramatically increases after aptamer immobilization (SH-Apt/MoS_2–N_2^+/SPE GPH, blue curve) and blocking with BSA (Blocker/SH-Apt/MoS_2–N_2^+/SPE GPH, purple curve). However, the incubation with the Spike protein causes a considerably decrease in the aptasensor response. This phenomenon can be explained by the formation of the folded conformation of the aptamer after the protein biorecognition, which could generate a steric hindrance that hinders the access of the $[Ru(bpy)_3]^{2+}$/TPrA system to the surface of the electrode and, as a result, the electron-transfer reaction. Consequently, the specific interaction between the aptamer and the analyte leads to a lower ECL signal than the one obtained for the blank. This effect was also previously described by our group [54] and will be employed to detect the highly specific protein-aptamer interaction.

3.2.4. Analytical performance study of the developed aptasensor

We studied the aptasensor response to different Spike protein concentrations, as is described in the experimental section. In order to avoid electrode to electrode variations, ECL signals were normalized to the signals obtained with blank (Blocker/SH-Apt/MoS_2–N_2^+/SPE GPH), following the next formula and the procedure explained in detail in

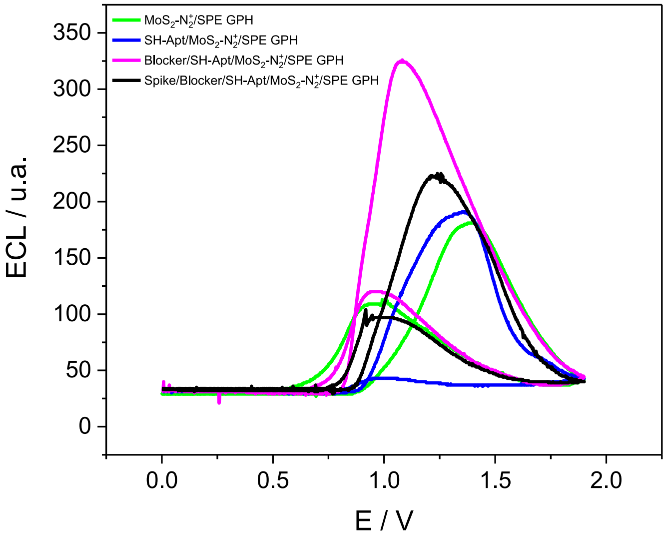

Fig. 4. ECL signals of MoS_2–N_2^+/SPE GPH (green curve), SH-Apt/MoS_2–N_2^+/SPE GPH (blue curve), Blocker/SH-Apt/MoS_2–N_2^+/SPE GPH (purple curve) and Spike (50.0 pg/mL)/Blocker/SH-Apt/MoS_2–N_2^+/SPE GPH (black curve) by using 7 mM $[Ru(bpy)_3]^{2+}$ with 500 μM TPrA in 0.1 M PB pH 7.4.

Experimental section:

$$\textit{Normalized ECL}\ (\%) = \frac{(\textit{ECL signal} - \textit{blank ECL signal})}{\textit{blank ECL signal}} \cdot 100$$

There is a linear relationship between the normalized ECL versus the logarithm of the Spike protein concentration (Fig. 5A). Thus, a calibration plot was obtained that fits the equation: Normalized ECL (%) = (11.5 ± 4.0) – (10.9 ± 1.1)·log[Spike] (R^2 = 0.9683). The limit of detection (LOD = $3 \cdot Sb \cdot m^{-1}$) and quantification (LOQ = $10 \cdot Sb \cdot m^{-1}$) (where m is the slope of the calibration plot and Sb is the standard deviation of the blank signal) were estimated to be 9.74 and 32.5 fg/mL, respectively, and the sensitivity 10.9 a.u. log(mL/fg).

To estimate the reproducibility of the aptasensor, we have quantified 5.00 pg/mL Spike protein with three different devices prepared in the exact same way, obtaining a relative standard deviation of 2.31 %.

Regarding the storage stability at 4 °C of the device, it was also evaluated (Fig. 5B). The aptasensor kept a 112.5 % of the initial ECL response for 30 days.

3.2.5. Selectivity study of the developed aptasensor

To evaluate the selectivity ECL aptasensor, we have tested other proteins (IgG, p53 and CEA) as potential interferences. For this purpose, we have recorded the ECL response of the aptasensor when it is exposed to the analyte (5.00 pg/mL Spike protein) in absence or presence of the selected interferences (5.00 pg/mL interference). As can be observed in Fig. 5C, all tested proteins do not have any interference on the detection of Spike protein, suggesting the great selectivity of the aptasensor even in the presence of these potential interferences.

3.2.6. Comparison between the response of the aptasensor developed and a commercial saliva antigen test

The applicability of the aptasensor was evaluated by applying it to the detection of the Spike protein in human saliva. The samples were prepared using untreated human saliva spiked with different concentrations of SARS-CoV-2 Spike protein. In particular, the same tested for the calibration plot (from 0.1 to 50.0 pg/mL), as is described in the experimental section and represented in Fig. 6A. The normalized ECL response of three aptasensors, prepared in the same way, were represented vs the log of Spike protein (Fig. 6A). As can be observed, when using saliva as a matrix, a linear trend is again obtained between the normalized ECL signal and the logarithm of the concentration, which verifies the possibility of applying the biosensor to human saliva samples without pretreatment. Furthermore, we have compared the sensitivity of our biosensor in the detection of SARS-CoV-2 virus in saliva samples versus that of a commercial antigen test for saliva samples. As can be seen in Fig. 6B, when the commercial antigen test is applied to human saliva samples with protein concentrations of the order of pg/mL, which is where the developed biosensor presents its linear range, negative results are obtained. Therefore, the commercial antigen test is less sensitive than our developed technology since it requires protein concentrations in the order of ng/mL to obtain positive results for SARS-CoV-2.

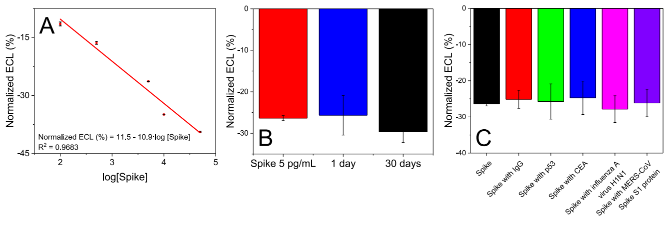

Fig. 5. (A) Calibration plot of the normalized ECL response (n = 3) of the developed biosensor vs log Spike concentration (from 0.10 pg/mL to 50.0 pg/mL). (B) Storage stability study at 4 °C of the Blocker/SH-Apt/MoS_2–N_2^+/SPE GPH platform. (C) Interference study. ECL aptasensor response (n = 3) of 5.00 pg/mL Spike without any interference (black bar), 5.00 pg/mL Spike and 5.00 pg/mL IgG (red bar), 5.00 pg/mL Spike and 5.00 pg/mL p53 (green bar), 5.00 pg/mL Spike and 5.00 pg/mL CEA (blue bar), 5.00 pg/mL Spike and 5.00 pg/mL Influenza A virus H1N1 (pink bar) and 5.00 pg/mL Spike and 5.00 pg/mL MERS-CoV Spike S1 protein (purple bar).

In terms of analysis time and cost, it is worth to note that the total time required for the detection of the SARS-CoV-2 virus in human saliva samples with the developed aptasensor is slightly longer than with the commercial antigen test (1 h versus 20 min), and the cost is also higher (8 euros (see budget in Table 2SI) versus 4,10 euros). However, the detection limit obtained with the aptasensor is much lower demonstrating the potential utility of this device even when the load viral of the disease is low.

Finally, we have compared the response of the aptasensor described in this work with other aptasensors recently reported in the literature for the detection of the Spike protein. At this point we would like to highlight that there is no other published aptasensor that uses the ECL technique for the transduction of the protein-aptamer biorecognition event. As can be seen in Table 1, when comparing the ECL aptasensor described in this work with others aptasensors prepared with different nanomaterials and transduction modes, we observe that our dispositive has a very competitive analytical parameters, with a superior LOD and linear range than the most of them. This fact allows us to suggest that the use of ECL in combination with the platform MoS_2–N_2^+/SPE GPH has a great potential in the development of novel biosensors for clinical diagnosis.

In conclusion, this ECL aptasensor represents a promising alternative tool for the selective detection of viral proteins as SARS-CoV-2 Spike protein. However, this methodology has a great versatility and could be extrapolated and applied to the diagnosis of other diseases and help control potential future outbreaks or pandemics.

4. Conclusions

A 2D covalent MoS_2/graphene heterostructured platform has been successfully applied to the development of an ECL aptasensor for the detection of the SARS-CoV-2 Spike protein. Thanks to this new methodology, this protein could be detected in a wide linear range (from 32.5 fg/mL to 50.0 pg/mL) with a low detection limit of 9.74 fg/mL. Moreover, this strategy presents high selectivity against other interfering proteins and huge applicability, after evaluating it applicability to identify the SARS-CoV-2 Spike protein in untreated human saliva samples. In conclusion, the ECL aptasensor developed based on the 2D covalent MoS_2/graphene heterostructure is a novel simple approach with a great potential for virus proteins detection.

Funding sources

This work has been financially supported by the Spanish Ministry of Economy and Competitiveness (PID2020-116728RB-I00, RED2022-134120-T) and Community of Madrid (TRANSNANOAVANSENS (S2018/NMT-4349) and FotoArt (P2018/NMT-4367)). E.M.P. acknowledges funding from the Ministerio de Ciencia, Innovación y Universidades (PID2020-116661RB-I00), and Comunidad de Madrid “Materiales Disruptivos Bidimensionales (2D)” (MAD2D-CM)-UAM and (MAD2D-CM)-IMDEA-NC funded by the Recovery, Transformation and Resilience Plan, and by NextGenerationEU from the European Union. IMDEA Nanoscience acknowledges support from the “Severo Ochoa'' Programme for Centres of Excellence in R&D CEX2020-001039-S. We also acknowledge the service from the MiNa Laboratory at IMN, and funding from CM (project S2018/NMT-4291 TEC2SPACE), MINECO (project CSIC13-4E-1794) and EU (FEDER, FSE).

CRediT authorship contribution statement

Laura Gutiérrez-Gálvez: Writing – review & editing, Writing – original draft, Methodology, Investigation, Formal analysis, Data curation, Conceptualization. **Hanaa El Hajioui-El Ghalbzouri:**

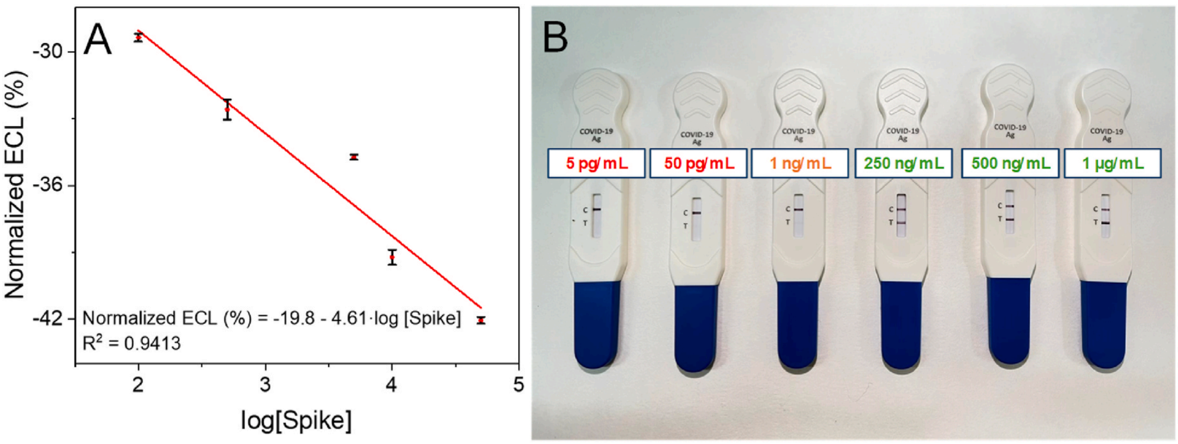

Fig. 6. (A) Calibration plot of the normalized ECL response (n = 3) of the developed biosensor vs log Spike concentration (from 0.10 pg/mL to 50.0 pg/mL) when using untreated human saliva samples. (B) Picture of the results obtained with the commercial antigen test at different protein concentrations (negative results are shown in red, the concentration at which the test appears to slightly detect the virus in orange and positive results in green).

Table 1
Aptasensors for spike protein detection. Abbreviatures: differential pulse voltammetry (DPV), chronopotentiometry (CP), photoelectrochemical (PEC), electrochemical impedance spectroscopy (EIS), high-frequency quartz crystal microbalance (HF-QCM) and hyperbranched rolling circle amplification (HRCA).

Principle	Transduction mode	Linear range	L.O.D.	Reference
A porous and flexible carbon cloth, coated with gold nanoparticles assembled with a thiol functionalized DNA aptamer	DPV CP	Until 1000 ng/mL	0.11 ng/mL 37.8 ng/mL	[14]
A two-dimensional metal-organic framework-based PEC aptasensor	PEC	0.5–8 μg/mL	72 ng/mL	[16]
$CeO_2@NH_2$ functionalized screen-printed carbon electrode	EIS	0.001–100 ng/mL	0.017 ng/mL	[21]
HF-QCM aptasensor	HF-QCM	0.001–1 ng/mL	0.25 pg/mL	[22]
2D MoS_2 and graphene heterostructure	EIS	7.01 to 200 fg/mL	2.10 fg/mL	[23]
An antibody-target-aptamer sandwich complex on the surface of microplates and elicits HRCA	Fluorescence	100 fg/mL to 1 μg/mL	89.7 fg/mL	[26]
2D MoS_2 and graphene heterostructure	ECL	32.5 fg/mL to 50.0 pg/mL	9.74 fg/mL	Present work

Investigation, Formal analysis, Data curation. **Estefanía Enebral-Romero:** Investigation, Formal analysis, Data curation. **Marina Garrido:** Investigation, Formal analysis, Data curation. **Alicia Naranjo:** Investigation, Formal analysis, Data curation. **David López-Diego:** Investigation, Formal analysis, Data curation. **Mónica Luna:** Writing – review & editing, Supervision, Resources, Project administration, Funding acquisition. **Emilio M. Pérez:** Writing – review & editing, Supervision, Resources, Project administration, Funding acquisition. **Tania García-Mendiola:** Writing – review & editing, Writing – original draft, Supervision, Resources, Project administration, Funding acquisition, Formal analysis, Data curation, Conceptualization. **Encarnación Lorenzo:** Writing – review & editing, Writing – original draft, Supervision, Resources, Project administration, Funding acquisition, Formal analysis, Data curation, Conceptualization.

Declaration of competing interest

The authors declare that they have no known competing financial interests or personal relationships that could have appeared to influence the work reported in this paper.

Data availability

Data will be made available on request.

Acknowledgment

The Spanish Ministry of Universities funded Laura Gutiérrez-Gálvez with a Formación del Profesorado Universitario (FPU) grant (FPU19/06309). Estefanía Enebral-Romero thank the financial support of “Nanotecnología para detección del SARS-CoV-2 y sus variants” project (NANOCOV-CM) and a contract as a predoctoral researcher funded by grant CEX2020-001039-S, supported by MCIN/AEI/10.13039/501100011033.

Appendix A. Supplementary data

Supplementary data to this article can be found online at https://doi.org/10.1016/j.talanta.2024.126293.

References

[1] W. Wang, S. Kang, W. Zhou, P.J. Vikesland, Environmental routes of virus transmission and the application of nanomaterial-based sensors for virus detection, Environ. Sci.: Nano 10 (2023) 393–423, https://doi.org/10.1039/D2EN00600F.
[2] F. Mirzadeh-rafie, F. Rahbarizadeh, N. Shoaei, F. Nasiri, M.R. Akbarizadeh, M. Khatami, Carbon nanoparticle-based COVID-19 biosensors, Sensors International 4 (2023) 100246, https://doi.org/10.1016/j.sintl.2023.100246.
[3] P.L. Truong, Y. Yin, D. Lee, S.H. Ko, Advancement in COVID-19 detection using nanomaterial-based biosensors, Explorations 3 (2023), https://doi.org/10.1002/EXP.20210232.
[4] Y.M. Aloraij, G.A.R.Y. Suaifan, A. Shibl, K. Al-Kattan, M.M. Zourob, Development of rapid aptamer-based screening assay for the detection of Covid-19 variants, ACS Omega (2023), https://doi.org/10.1021/acsomega.3c04137.
[5] Y. Zhang, M. Juhas, C.K. Kwok, Aptamers targeting SARS-COV-2: a promising tool to fight against COVID-19, Trends Biotechnol. 41 (2023) 528–544, https://doi.org/10.1016/j.tibtech.2022.07.012.
[6] F.R.W. Schmitz, K. Cesca, A. Valério, D. de Oliveira, D. Hotza, Colorimetric detection of Pseudomonas aeruginosa by aptamer-functionalized gold nanoparticles, Appl. Microbiol. Biotechnol. 107 (2023) 71–80, https://doi.org/10.1007/s00253-022-12283-5.
[7] Y. Zhang, Y. Liu, Y. Yang, L. Li, X. Tao, E. Song, Rapid detection of pathogenic bacteria based on a universal dual-recognition FRET sensing system constructed

with aptamer-quantum dots and lectin-gold nanoparticles, Chin. Chem. Lett. 34 (2023) 108102, https://doi.org/10.1016/j.cclet.2022.108102.

[8] F. Davodabadi, S. Mirinejad, S. Fathi-Karkan, M. Majidpour, N. Ajalli, R. Sheervalilou, S. Sargazi, D. Rozmus, A. Rahdar, A.M. Diez-Pascual, Aptamer-functionalized quantum dots as theranostic nanotools against cancer and bacterial infections: a comprehensive overview of recent trends, Biotechnol. Prog. (2023), https://doi.org/10.1002/btpr.3366.

[9] M. Vargas-Montes, N. Cardona, D.M. Moncada, D.A. Molina, Y. Zhang, J.E. Gómez-Marín, Enzyme-linked aptamer assay (ELAA) for detection of toxoplasma ROP18 protein in human serum, Front. Cell. Infect. Microbiol. 9 (2019), https://doi.org/10.3389/fcimb.2019.00386.

[10] N.E. Brosseau, I. Vallée, A. Mayer-Scholl, M. Ndao, G. Karadjian, Aptamer-based technologies for parasite detection, Sensors 23 (2023) 562, https://doi.org/10.3390/s23020562.

[11] X. Liu, X. Chen, Y. Dong, C. Zhang, X. Qu, Y. Lei, Z. Jiang, X. Wei, Multiple virus sorting based on aptamer-modified microspheres in a TSAW device, Microsyst Nanoeng 9 (2023) 64, https://doi.org/10.1038/s41378-023-00523-1.

[12] S. Ma, Q. Ren, L. Jiang, Z. Liu, Y. Zhu, J. Zhu, Y. Zhang, M. Zhang, A triple-aptamer tetrahedral DNA nanostructures based carbon-nanotube-array transistor biosensor for rapid virus detection, Talanta 266 (2024) 124973, https://doi.org/10.1016/j.talanta.2023.124973.

[13] W. Ma, W. Xie, R. Tian, X. Zeng, L. Liang, C. Hou, D. Huo, D. Wang, An ultrasensitive aptasensor of SARS-CoV-2 N protein based on ion current rectification with nanopipettes, Sensor. Actuator. B Chem. 377 (2023) 133075, https://doi.org/10.1016/j.snb.2022.133075.

[14] M. Adeel, K. Asif, F. Alshabouna, V. Canzonieri, MdM. Rahman, S.A. Ansari, F. Güder, F. Rizzolio, S. Daniele, Label-free electrochemical aptasensor for the detection of SARS-CoV-2 spike protein based on carbon cloth sputtered gold nanoparticles, Biosens. Bioelectron. X 12 (2022) 100256, https://doi.org/10.1016/j.biosx.2022.100256.

[15] H. Chen, S.-G. Park, N. Choi, H.-J. Kwon, T. Kang, M.-K. Lee, J. Choo, Sensitive detection of SARS-CoV-2 using a SERS-based aptasensor, ACS Sens. 6 (2021) 2378–2385, https://doi.org/10.1021/acssensors.1c00596.

[16] Z.W. Jiang, T.T. Zhao, C.M. Li, Y.F. Li, C.Z. Huang, 2D MOF-based photoelectrochemical aptasensor for SARS-CoV-2 spike glycoprotein detection, ACS Appl. Mater. Interfaces 13 (2021) 49754–49761, https://doi.org/10.1021/acsami.1c17574.

[17] E. Zavyalova, O. Ambartsumyan, G. Zhdanov, D. Gribanyov, V. Gushchin, A. Tkachuk, E. Rudakova, M. Nikiforova, N. Kuznetsova, L. Popova, B. Verdiev, A. Alatyrev, E. Burtseva, A. Ignatieva, A. Iliukhina, I. Dolzhikova, A. Arutyunyan, A. Gambaryan, V. Kukushkin, SERS-based aptasensor for rapid quantitative detection of SARS-CoV-2, Nanomaterials 11 (2021) 1394, https://doi.org/10.3390/nano11061394.

[18] F. Curti, S. Fortunati, W. Knoll, M. Giannetto, R. Corradini, A. Bertucci, M. Careri, A folding-based electrochemical aptasensor for the single-step detection of the SARS-CoV-2 spike protein, ACS Appl. Mater. Interfaces 14 (2022) 19204–19211, https://doi.org/10.1021/acsami.2c02405.

[19] C. Han, W. Xing, W. Li, X. Fang, J. Zhao, F. Ge, W. Ding, P. Qu, Z. Luo, L. Zhang, Aptamers dimerization inspired biomimetic clamp assay towards impedimetric SARS-CoV-2 antigen detection, Sensor. Actuator. B Chem. 380 (2023) 133387, https://doi.org/10.1016/j.snb.2023.133387.

[20] K.S. Park, A. Choi, H.J. Kim, I. Park, M.-S. Eom, S.-G. Yeo, R.G. Son, T.-I. Park, G. Lee, H.T. Soh, Y. Hong, S.P. Pack, Ultra-sensitive label-free SERS biosensor with high-throughput screened DNA aptamer for universal detection of SARS-CoV-2 variants from clinical samples, Biosens. Bioelectron. 228 (2023) 115202, https://doi.org/10.1016/j.bios.2023.115202.

[21] A. Triastuti, S.N. Zakiyyah, S. Gaffar, I. Anshori, A. Surawijaya, D. Hidayat, H. L. Wiraswati, M. Yusuf, Y.W. Hartati, CeO_2 @NH_2 functionalized electrodes for the rapid detection of SARS-CoV-2 spike receptor binding domain, RSC Adv. 13 (2023) 5874–5884, https://doi.org/10.1039/D2RA07560A.

[22] Q. Zhang, S. Liu, X. Zhang, C. Du, S. Si, J. Chen, A high-frequency QCM biosensing platform for label-free detection of the SARS-CoV-2 spike receptor-binding domain: an aptasensor and an immunosensor, Analyst 148 (2023) 719–723, https://doi.org/10.1039/D3AN00008G.

[23] E. Enebral-Romero, L. Gutiérrez-Gálvez, R. Del Caño, M.V. Sulleiro, A. Naranjo, I. J. Gómez, F. Pariente, E.M. Pérez, T. García-Mendiola, E. Lorenzo, Pathogen sensing device based on 2D MoS2/graphene heterostructure, Sensor. Actuator. B Chem. 392 (2023) 134105, https://doi.org/10.1016/j.snb.2023.134105.

[24] Y. Xie, Q. Li, J. Chen, W. Yue, Z. Xia, M. Zeng, Y. He, Y. Zhao, X. Luo, Sensitive SERS detection of SARS-CoV-2 spike protein based on Y-shaped-aptasensor and AuNPs/COFs composites, Sensor. Actuator. B Chem. 394 (2023) 134470, https://doi.org/10.1016/j.snb.2023.134470.

[25] G. Moreira, H. Qian, S.P.A. Datta, N. Bliznyuk, J. Carpenter, D. Dean, E. McLamore, D. Vanegas, A capacitive laser-induced graphene based aptasensor for SARS-CoV-2 detection in human saliva, PLoS One 18 (2023) e0290256, https://doi.org/10.1371/journal.pone.0290256.

[26] Z. Wang, C. Zhang, S. He, D. Xu, An ultrasensitive fluorescence aptasensor for SARS-CoV-2 antigen based on hyperbranched rolling circle amplification, Talanta 255 (2023) 124221, https://doi.org/10.1016/j.talanta.2022.124221.

[27] R. Luo, D. Zhu, H. Ju, J. Lei, Reticular electrochemiluminescence nanoemitters: structural design and enhancement mechanism, Acc. Chem. Res. 56 (2023) 1920–1930, https://doi.org/10.1021/acs.accounts.3c00145.

[28] A. Barhoum, Z. Altintas, K.S.S. Devi, R.J. Forster, Electrochemiluminescence biosensors for detection of cancer biomarkers in biofluids: principles, opportunities, and challenges, Nano Today 50 (2023) 101874, https://doi.org/10.1016/j.nantod.2023.101874.

[29] R. Ahmad, O.S. Wolfbeis, Y.-B. Hahn, H.N. Alshareef, L. Torsi, K.N. Salama, Deposition of nanomaterials: a crucial step in biosensor fabrication, Mater. Today Commun. 17 (2018) 289–321, https://doi.org/10.1016/j.mtcomm.2018.09.024.

[30] A.A. Ibrahim, R. Ahmad, A. Umar, M.S. Al-Assiri, A.E. Al-Salami, R. Kumar, S. G. Ansari, S. Baskoutas, Two-dimensional ytterbium oxide nanodisks based biosensor for selective detection of urea, Biosens. Bioelectron. 98 (2017) 254–260, https://doi.org/10.1016/j.bios.2017.06.015.

[31] L. Wang, X. Lu, C. Wen, Y. Xie, L. Miao, S. Chen, H. Li, P. Li, Y. Song, One-step synthesis of Pt–NiO nanoplate array/reduced graphene oxide nanocomposites for nonenzymatic glucose sensing, J Mater Chem A Mater 3 (2015) 608–616, https://doi.org/10.1039/C4TA04724A.

[32] A.T. Lawal, Progress in utilisation of graphene for electrochemical biosensors, Biosens. Bioelectron. 106 (2018) 149–178, https://doi.org/10.1016/j.bios.2018.01.030.

[33] S. Shrivastava, N. Jadon, R. Jain, Next-generation polymer nanocomposite-based electrochemical sensors and biosensors: a review, TrAC, Trends Anal. Chem. 82 (2016) 55–67, https://doi.org/10.1016/j.trac.2016.04.005.

[34] K. Tian, M. Prestgard, A. Tiwari, A review of recent advances in nonenzymatic glucose sensors, Mater. Sci. Eng. C 41 (2014) 100–118, https://doi.org/10.1016/j.msec.2014.04.013.

[35] D. Voiry, A. Goswami, R. Kappera, C. de C.C. e Silva, D. Kaplan, T. Fujita, M. Chen, T. Asefa, M. Chhowalla, Covalent functionalization of monolayered transition metal dichalcogenides by phase engineering, Nat. Chem. 7 (2015) 45–49, https://doi.org/10.1038/nchem.2108.

[36] M. Vera-Hidalgo, E. Giovanelli, C. Navío, E.M. Pérez, Mild covalent functionalization of transition metal dichalcogenides with maleimides: a "click" reaction for 2H-MoS_2 and WS_2, J. Am. Chem. Soc. 141 (2019) 3767–3771, https://doi.org/10.1021/jacs.8b10930.

[37] S. Bertolazzi, M. Gobbi, Y. Zhao, C. Backes, P. Samorì, Molecular chemistry approaches for tuning the properties of two-dimensional transition metal dichalcogenides, Chem. Soc. Rev. 47 (2018) 6845–6888, https://doi.org/10.1039/C8CS00169C.

[38] X. Chen, C. McGlynn, A.R. McDonald, Two-Dimensional MoS2 catalyzed oxidation of organic thiols, Chem. Mater. 30 (2018) 6978–6982, https://doi.org/10.1021/ACS.CHEMMATER.8B01454/ASSET/IMAGES/LARGE/CM-2018-01454J_0005. JPEG.

[39] R. Canton-Vitoria, Y. Sayed-Ahmad-Baraza, M. Pelaez-Fernandez, R. Arenal, C. Bittencourt, C.P. Ewels, N. Tagmatarchis, Functionalization of MoS2 with 1,2-dithiolanes: toward donor-acceptor nanohybrids for energy conversion, NPJ 2D Mater Appl 1 (2017) 13, https://doi.org/10.1038/s41699-017-0012-8.

[40] R. Quirós-Ovies, M. Vázquez Sulleiro, M. Vera-Hidalgo, J. Prieto, I.J. Gómez, V. Sebastián, J. Santamaría, E.M. Pérez, Controlled covalent functionalization of 2 H-MoS_2 with molecular or polymeric adlayers, Chem. Eur J. 26 (2020) 6629–6634, https://doi.org/10.1002/chem.202000068.

[41] J. Miao, L. Wu, Z. Bian, Q. Zhu, T. Zhang, X. Pan, J. Hu, W. Xu, Y. Wang, Y. Xu, B. Yu, W. Ji, X. Zhang, J. Qiao, P. Samorì, Y. Zhao, A "click" reaction to engineer MoS_2 field-effect transistors with low contact resistance, ACS Nano 16 (2022) 20647–20655, https://doi.org/10.1021/acsnano.2c07670.

[42] T. Talha-Dean, K. Chen, G. Mastroianni, F. Gesuele, J. Mol, M. Palma, Nanoscale control of DNA-linked MoS_2 -quantum dot heterostructures, Bioconjugate Chem. 34 (2023) 78–84, https://doi.org/10.1021/acs.bioconjchem.2c00285.

[43] M. Vázquez Sulleiro, A. Develioglu, R. Quirós-Ovies, L. Martín-Pérez, N. Martín Sabanés, M.L. Gonzalez-Juarez, I.J. Gómez, M. Vera-Hidalgo, V. Sebastián, J. Santamaría, E. Burzurí, E.M. Pérez, Fabrication of devices featuring covalently linked MoS2-graphene heterostructures, Nat. Chem. 14 (2022) 695–700, https://doi.org/10.1038/S41557-022-00924-1.

[44] E. Martínez-Periñán, T. García-Mendiola, E. Enebral-Romero, R. del Caño, M. Vera-Hidalgo, M. Vázquez Sulleiro, C. Navío, F. Pariente, E.M. Pérez, E. Lorenzo, A MoS2 platform and thionine-carbon nanodots for sensitive and selective detection of pathogens, Biosens. Bioelectron. 189 (2021) 113375, https://doi.org/10.1016/J.BIOS.2021.113375.

[45] D. Jariwala, V.K. Sangwan, L.J. Lauhon, T.J. Marks, M.C. Hersam, Emerging device applications for semiconducting two-dimensional transition metal dichalcogenides, ACS Nano 8 (2014) 1102–1120, https://doi.org/10.1021/NN500064S/ASSET/IMAGES/LARGE/NN-2014-00064S_0010. JPEG.

[46] A. Tuxen, J. Kibsgaard, H. Gøbel, E. Lægsgaard, H. Topsøe, J.V. Lauritsen, F. Besenbacher, Size threshold in the dibenzothiophene adsorption on MoS2 nanoclusters, ACS Nano 4 (2010) 4677–4682, https://doi.org/10.1021/NN1011013/SUPPL_FILE/NN1011013_SI_001.PDF.

[47] Q.H. Wang, K. Kalantar-Zadeh, A. Kis, J.N. Coleman, M.S. Strano, Electronics and optoelectronics of two-dimensional transition metal dichalcogenides, Nat. Nanotechnol. 7 (2012) 699–712, https://doi.org/10.1038/NNANO.2012.193.

[48] I. Horcas, R. Fernández, J.M. Gómez-Rodríguez, J. Colchero, J. Gómez-Herrero, A. M. Baro, WSXM: a software for scanning probe microscopy and a tool for nanotechnology, Rev. Sci. Instrum. 78 (2007) 013705, https://doi.org/10.1063/1.2432410.

[49] D.C. Ferreira, M.R. Batistuti, B. Bachour, M. Mulato, Aptasensor based on screen-printed electrode for breast cancer detection in undiluted human serum, Bioelectrochemistry 137 (2021) 107586, https://doi.org/10.1016/J.BIOELECHEM.2020.107586.

[50] J. Pinson, F. Podvorica, Attachment of organic layers to conductive or semiconductive surfaces by reduction of diazonium salts, Chem. Soc. Rev. 34 (2005) 429–439, https://doi.org/10.1039/B406228K.

[51] M. Sornambigai, L. Bouffier, N. Sojic, S.S. Kumar, Tris(2,2'-bipyridyl)ruthenium (II) complex as a universal reagent for the fabrication of heterogeneous

electrochemiluminescence platforms and its recent analytical applications, Anal. Bioanal. Chem. (2023), https://doi.org/10.1007/s00216-023-04876-4.

[52] L. Hu, G. Xu, Applications and trends in electrochemiluminescence, Chem. Soc. Rev. 39 (2010) 3275, https://doi.org/10.1039/b923679c.

[53] C.P. Kurup, N.F. Mohd-Naim, M.U. Ahmed, A solid-state electrochemiluminescence aptasensor for β-lactoglobulin using Ru-AuNP/GNP/Naf nanocomposite-modified printed sensor, Microchim. Acta 189 (2022) 165, https://doi.org/10.1007/s00604-022-05275-9.

[54] L. Gutiérrez-Gálvez, M.V. Sulleiro, C. Gutiérrez-Sánchez, D. García-Nieto, M. Luna, E.M. Pérez, T. García-Mendiola, E. Lorenzo, MoS2-Carbon nanodots as a new electrochemiluminescence platform for breast cancer biomarker detection, Biosensors 13 (2023) 348, https://doi.org/10.3390/bios13030348.

[55] Y.M. Liu, G.F. Shi, J.J. Zhang, M. Zhou, J.T. Cao, K.J. Huang, S.W. Ren, A novel label-free electrochemiluminescence aptasensor based on layered flowerlike molybdenum sulfide–graphene nanocomposites as matrix, Colloids Surf. B Biointerfaces 122 (2014) 287–293, https://doi.org/10.1016/J.COLSURFB.2014.07.011.

[56] L. Fan, G. Zhao, H. Shi, M. Liu, Z. Li, A highly selective electrochemical impedance spectroscopy-based aptasensor for sensitive detection of acetamiprid, Biosens. Bioelectron. 43 (2013) 12–18, https://doi.org/10.1016/J.BIOS.2012.11.033.

[57] J.C. Abrego-Martinez, M. Jafari, S. Chergui, C. Pavel, D. Che, M. Siaj, Aptamer-based electrochemical biosensor for rapid detection of SARS-CoV-2: nanoscale electrode-aptamer-SARS-CoV-2 imaging by photo-induced force microscopy, Biosens. Bioelectron. 195 (2022) 113595, https://doi.org/10.1016/J.BIOS.2021.113595.

[58] S. Mehennaoui, S. Poorahong, G.C. Jimenez, M. Siaj, Selection of high affinity aptamer-ligand for dexamethasone and its electrochemical biosensor, Sci. Rep. 9 (1 9) (2019) 1–9, https://doi.org/10.1038/s41598-019-42671-3, 2019.

[59] Y.M. Liu, G.F. Shi, J.J. Zhang, M. Zhou, J.T. Cao, K.J. Huang, S.W. Ren, A novel label-free electrochemiluminescence aptasensor based on layered flowerlike molybdenum sulfide–graphene nanocomposites as matrix, Colloids Surf. B Biointerfaces 122 (2014) 287–293, https://doi.org/10.1016/J.COLSURFB.2014.07.011.

[60] K.C. Lin, B. Jagannath, S. Muthukumar, S. Prasad, Sub-picomolar label-free detection of thrombin using electrochemical impedance spectroscopy of aptamer-functionalized MoS2, Analyst 142 (2017) 2770–2780, https://doi.org/10.1039/C7AN00548B.